Mem. S.A.It. Vol. 88, 37

Memorie della

CO5BOLD for MHD: progresses and deficiencies

O. Steiner[1,2], F. Calvo[2,3], R. Salhab[1], and G. Vigeesh[1]

[1] Kiepenheuer-Institut für Sonnenphysik, Schöneckstrasse 6, 79104 Freiburg i. Br., Germany
e-mail: steiner@leibniz-kis.de
[2] Istituto Ricerche Solari Locarno (IRSOL), via Patocchi 57—Prato Pernice, 6605 Locarno-Monti, Switzerland
[3] Geneva Observatory, University of Geneva, chem. des Maillettes 51, 1290 Sauverny, Switzerland

Abstract. The magnetohydrodynamics module of CO5BOLD has been steadily improved over the past decade and has been used for various solar and stellar physical applications. We give an overview of current work with it and of remaining and newly emerged shortcomings.

Key words. Magnetohydrodynamics (MHD) – Methods: numerical – Convection – Sun: atmosphere — Sun: magnetic fields — Stars: atmospheres – Stars: magnetic fields

1. Introduction

The MHD module of CO5BOLD exists since 2005 (Schaffenberger et al. 2005, 2006). It is based on the HLL approximate Riemann solver in the implementation for MHD of Janhunen (2000) (see also Freytag et al. 2012). At the beginning, we used HLLMHD in combination with the van Leer reconstruction scheme, which proved to be overly diffusive. In the course of the second CO5BOLD-workshop, we reported under the title "First steps with HLLMHD and PP reconstruction" on progresses with a piecewise parabolic, less diffuse scheme (Steiner et al. 2013). This concerned code version `002.00.2011.04.28`.

Meanwhile, we are using the code version `002.02.2012.11.05f` and instead of PP, we use the FRweno reconstruction scheme (Freytag 2013). This version and reconstruction scheme solves all the problems of the MHD module reported during the second CO5BOLD-workshop. In particular:

(i) wiggles, saw-teeth, and single cells of very low temperature in horizontal sections at chromospheric heights;
(ii) strong oscillations in intensity and mass flux of certain models;
(iii) wiggles in the vertical mass flux as a function of height.

Problem (i) got solved with the introduction of FRweno, and problems (ii) and (iii) got solved with a bug fix concerning the Hancock time-integration scheme.

A detailed account on these problems and their resolution is given in a series of KIS internal reports "First steps with HLLMHD and PP reconstruction", part I–V, available from the corresponding author.

2. Current work with MHD-CO5BOLD at KIS and IRSOL

At the Kiepenheuer-Institut (KIS), we are presently running 15 different stellar atmo-

Table 1. Basic characteristics of the stellar MHD simulations currently carried out at KIS. Each of these models is run with an initial homogeneous vertical magnetic field of flux density 50 G (v50) and 100 G (v100), and magnetic field-free. All models have been run for 10.5 h physical time with the exception of the model with $T^*_{\rm eff}$ = 3300 K and the 100 G models, which have not yet reached this time. $T^*_{\rm eff}$ is the nominal (target) temperature. For the field-free and the v50 models, the actual temporal mean effective temperature differs from $T^*_{\rm eff}$ by less than 1 %.

model name	$T^*_{\rm eff}$	$\log g$	$X \times Y \times Z$ [km^3]	$\Delta_{x,y}$	Δ_z	$N_x \times N_y \times N_z$
d3t33g45[v50,v100]rs	3300	4.5	$2394 \times 2394 \times 1629$	4.5	4.5	$532 \times 532 \times 362$
d3t40g45[v50,v100]rs	4000	4.5	$4734 \times 4734 \times 1232$	9.0	7.0	$526 \times 526 \times 176$
d3t50g45[v50,v100]rs	5000	4.5	$4928 \times 4928 \times 2484$	11.0	9.0	$448 \times 448 \times 276$
d3gt57g44[v50,v100]rs	5770	4.44	$5600 \times 5600 \times 2256$	14.0	12.0	$400 \times 400 \times 188$
d3t65g45[v50,v100]rs	6500	4.5	$8388 \times 8388 \times 4020$	18.0	15.0	$466 \times 466 \times 268$

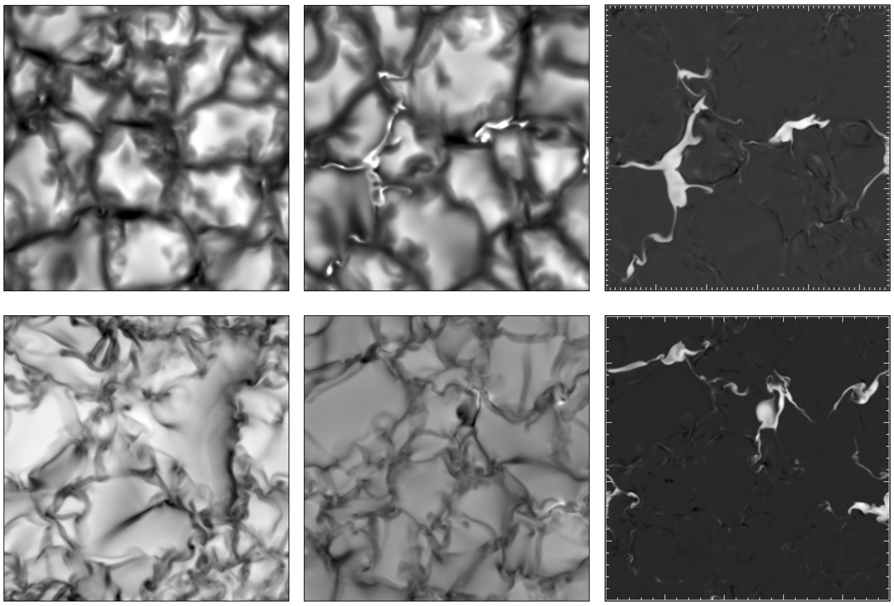

Fig. 1. Example snapshots of runs listed in Table 1. *Top row:* solar model d3gt57g44[v50]rs. *Bottom row:* model d3t33g45[v50]rs with effective temperature $T^*_{\rm eff}$ = 3300 K. Columns from *left to right* show the emergent bolometric radiative intensity of the magnetic field-free models, the emergent bolometric radiative intensity of the models with magnetic fields, and the vertical component of the magnetic field at the average height level of the surface of Rosseland optical depth $\tau_{\rm R}$ = 1. Grayscales range from minimal to maximal value for each individual panel. The magnetic field strength ranges from −480 G *(black)* to 1770 G *(white)* in the top right panel and from −460 G to 2110 G in the bottom right panel. Horizontal dimensions are given in Table 1.

spheric simulations for five different spectral types. For each spectral type, we start the simulation once with an initial homogeneous vertical magnetic field of a flux density of 50 G, once of 100 G, and once without a magnetic field but using the very same HLLMHD solver that is used for the magnetic runs and with the very same boundary conditions. The details of the boundary conditions will be explained in a forthcoming paper about these simulation runs

Table 2. Basic characteristics of the solar MHD simulations currently carried out at KIS for investigating gravity wave propagation. Simulations with an initial homogenous magnetic field of 50 G flux density in strictly vertical and strictly horizontal direction have been carried out in conjunction with a field-free simulation, all with the very same solver, numerical parameters, and boundary conditions.

model name	$T^*_{\rm eff}$	$\log g$	$X \times Y \times Z$ [km^3]	$\Delta_{x,y}$	Δ_z	$N_x \times N_y \times N_z$	$B_{\rm init}$ [G]	t [h]
d3t57g45gv	5770	4.44	$38\,400 \times 38\,400 \times 2800$	80	20–50	$480 \times 480 \times 120$	0	8.0
d3t57g45v50gv							$B_z = 50$	8.0
d3t57g45uh50gv							$B_x = 50$	3.0

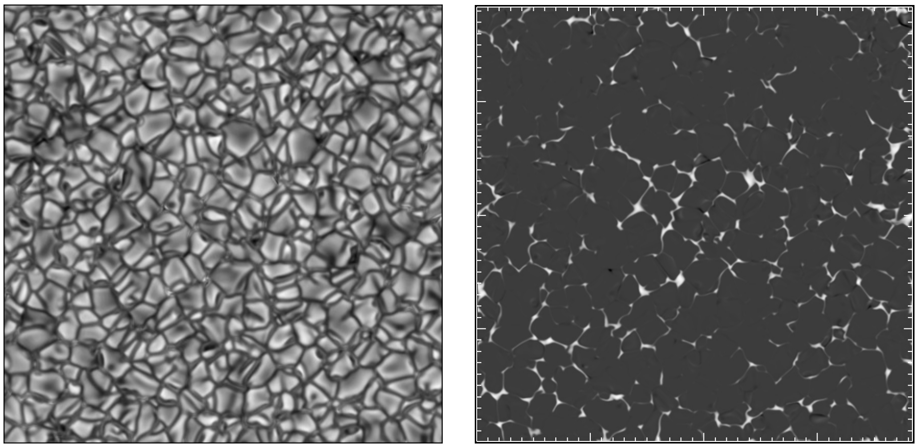

Fig. 2. Time instant of simulation d3t57g45v50gv showing *(left)* the emergent bolometric intensity and *(right)* the vertical component of the magnetic field at $\langle z(\tau_{\rm R} = 1)\rangle$. In the panel on the right, the grayscales range from -500 G *(black)* to 1600 G *(white)*. For the horizontal dimensions see Table 2.

by Salhab et al. (2017); a brief explanation is provided in Steiner et al. (2014).

Some basic characteristics of the models are given in Table 1. We note that the net (signed) magnetic flux is fixed by the initial condition and stays constant with time.

First ideas regarding this work were presented at the second CO5BOLD workshop (Steiner et al. 2013) and first results were published in Steiner et al. (2014). Presently, we are preparing an in depth paper on the subject in which we analyze the models from $T^*_{\rm eff} = 4000$ K to $T^*_{\rm eff} = 6500$ K, corresponding to spectral types K8V to F5V. Comparing the magnetic field-free models with the corresponding models with initial field strength of 50 G, we find that in the (spatial and temporal) average, the vertically directed bolometric intensity at the top boundary of the magnetic model always surpasses that of the non-magnetic model for all spectral types. This radiative surplus of the magnetic model is most pronounced for the solar model, where it amounts to 0.8%. It is also prominent in case of the K2V model (0.66%) but sharply drops to smaller values for hotter and cooler atmospheres. The radiative surplus of the magnetic models is even more prominent in the vertically directed radiative flux: 1.0% for the solar model. This increase is due to the "hot wall effect" of small-scale magnetic flux concentrations, which render them particularly bright when seen under an inclined angle with respect to the vertical direction.

Figure 1 shows example snapshots of the solar model (d3gt57g44[v50]rs, top row pan-

Table 3. Basic characteristics of the solar MHD simulations currently carried out at IRSOL.

model name	$T^*_{\rm eff}$	$\log g$	$X \times Y \times Z$ [km^3]	$\Delta_{x,y}$	Δ_z	$N_x \times N_y \times N_z$	t [h]
d3t57g45[...]fc	5770	4.44	$9600 \times 9600 \times 2800$	10	10	$960 \times 960 \times 280$	2.0

model name	solver	initial magnetic field configuration	t [h]
d3t57g45roefc	Roe	no magnetic field	4.1
d3t57g45b0fc	HLLMHD	no magnetic field	3.5
d3t57g45v50fc	HLLMHD	vertical, homogeneous, 50 G	1.9
d3t57g45v200fc	HLLMHD	vertical, homogeneous, 200 G	3.2
d3t57g45h50fc	HLLMHD	horizontally inflowing, 50 G	3.0
d3t57g45p200fc	HLLMHD	potential filed configuration	0.5

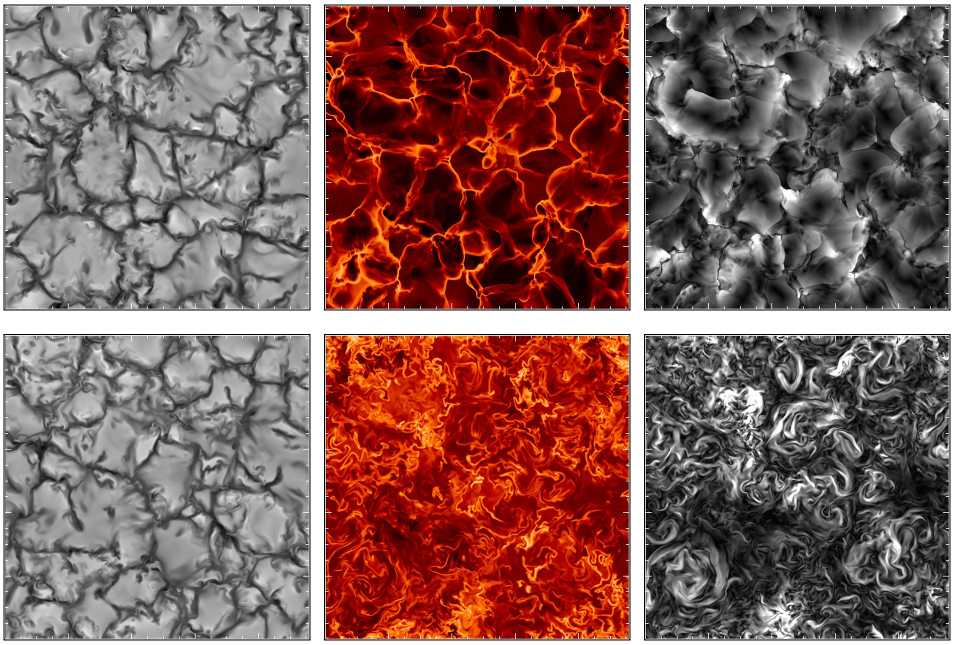

Fig. 3. Example snapshots of *(top row)* the magnetic field-free run d3t57g45b0fc and of *(bottom row)* the magnetic run d3t57g45v50fc (see Table 3). The panels in the *first column* show the vertical velocity at $\langle z(\tau_R = 1)\rangle$, in the *middle column* the temperature in the horizontal section 1200 km above the mean optical depth $\tau_{\rm R} = 1$, and, at the same height, in the *right column*, the horizontal velocity. Gray- and color scales range for the vertical velocity from -10 to $+10\,{\rm km\,s^{-1}}$, for the temperature from 2000 to 7000 K, and for the horizontal velocity from 0.0 to $15\,{\rm km\,s^{-1}}$ in the upper panel and from 0.0 to $25\,{\rm km\,s^{-1}}$ in the lower panel.

els) and the model with effective temperature $T^*_{\rm eff} = 3300$ K (d3t33g45[v50]rs, bottom row panels). Displayed from left to right are the emergent radiative intensity of the magnetic field-free model, the emergent intensity of the model with magnetic field, and the vertical component of the magnetic field strength at the average height level of the surface of Rosseland optical depth $\tau_{\rm R} = 1$. While all the magnetic flux concentrations of the solar model appear bright in the intensity map, some are dark in the model with $T^*_{\rm eff} = 3300$ K, like the concentration in the upper right direction from the center, and in the upper left corner.

Also at KIS, G. Vigeesh has run a model of large surface area of $38.4\times38.4\,\mathrm{Mm}^2$, with and without magnetic field. Some basic characteristics of these models are given in Table 2. He uses these models for studying gravity waves, in particular the differences in the propagation of gravity waves between the magnetic and the non-magnetic model (Vigeesh et al. 2017a,b). The principal result is that the propagation of gravity waves from the photosphere into higher layers of the atmosphere is suppressed by the presence of vertically directed magnetic fields because of mode conversion. Fig. 2 gives an impression of the size of the model.

At the Istituto Ricerche Solari Locarno (IRSOL), we are running high resolution solar models (grid size 10 km) with and without magnetic field and of various initial field configurations. Computations were carried out on Piz Dora, a Cray XC40 computer (1256 nodes, 24 cores per node) at the Swiss National Supercomputing Center, CSCS. Characteristics of the model runs are given in Table 3. Fig. 3 shows snapshots from the magnetic field-free run d3t57g45b0fc in the top row of panels and from the magnetic run d3t57g45v50fc in the bottom row. Although the two models look very similar in the photosphere (first column of Fig. 3), at chromospheric heights, the temperature distribution and flow field are drastically different. While the non-magnetic run shows shock fronts with cells of divergent flows (see also Wedemeyer et al. 2004), the magnetic run is marked by vortical flows and a small-scale structure in temperature, with the shock fronts being less prominent than in the field-free case (see Steiner & Rezaei 2012, for more details). The vortical flows are generated by magnetic fields whose footpoints are trapped and move with corresponding flows in the surface layers of the convection zone.

These simulations are used at IRSOL for *(i)* the determination of statistical properties of non-magnetic bright points, *(ii)* a study of Stokes-V line ratios, and *(iii)* the computation of the center-to-limb variation of the continuum polarization. Details on the non-magnetic bright points can be found in Calvo et al. (2016). The principal result is that tiny bright points appear within intergranular lanes that are not due to magnetic flux concentrations but are due to swirling downdrafts that form a funnel of reduced density owing to the centrifugal force.

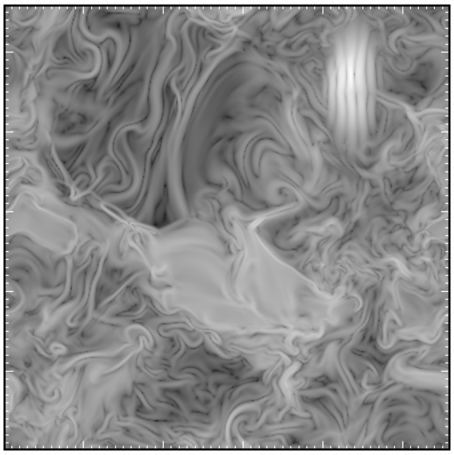

Fig. 4. Instance of the development of a numerical instability at the top boundary of a solar model. Grayscales indicate the logarithm of the absolute electric current density in the topmost horizontal section. The instability appears near the upper right corner of the section. The horizontal dimensions are $5.6\times5.6\,\mathrm{Mm}$.

3. Unresolved problems with MHD-CO5BOLD

Despite the significant progress that we achieved with the MHD module of CO5BOLD in recent years, there also exist a number of deficiencies and wish-list items, which are briefly discussed in the following.

3.1. B-field instability near the top

Occasionally, we experienced the development of an instability that occurs near the top boundary, obviously due to the magnetic field. It is best seen in the electric current density as a peculiar pattern aligned with one and the same coordinate axis. A typical example is shown in Fig. 4 (upper right corner). The instability arises most likely from the constrained transport of the magnetic field. A bug fix in the computation of the Courant-Friedrichs-Lewy (CFL) conditional time step has mitigated the problem but did not entirely eliminate it. Presently, the best remedy consists in reducing the time step by setting the parameter `c_courant` = 0.5 for runs with the HLLMHD solver. With this measure, the problem did not reoccur.

3.2. Very slowly growing instability

A continuing problem of the MHD module that was already mentioned in part V of the internal report "First steps with HLLMHD and PP reconstruction" referred to in Sect. 1 poses the occasional development of a very slowly growing instability that may take several hours of physical time until it becomes apparent. Fig. 5 displays the radiative flux across the top boundary in units of $\sigma T_{\mathrm{eff}}^{*4}$ for a model with effective temperature $T_{\mathrm{eff}}^{*} = 4000\,\mathrm{K}$ and $\log g = 4.5$. In this case and examining this quantity alone, the instability becomes only visible after more than 4 h physical time. It becomes a bit sooner visible when plotting the horizontally averaged mean mass flux as a function of time at, say, $\tau_{\mathrm{R}} = 1$. The problem seems to occur more frequently for cool stellar atmospheres than for the Sun and warmer models but we also experienced it for a solar model of large horizontal extension (d3t57g45gv, see Fig. 6) and it is not exclusive of the MHD solver. In fact, changing the (M)HD solver or the time integration scheme does not fix the problem; it seems to pertain to the hydrodynamic lower boundary condition alone.

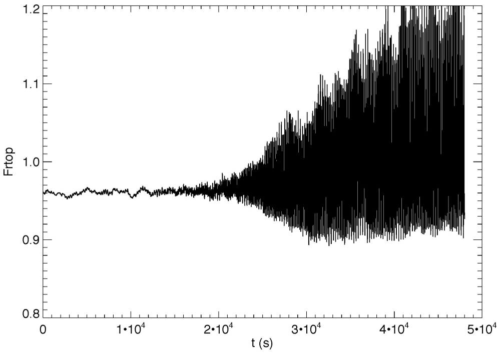

Fig. 5. Radiative flux across the top boundary in units of $\sigma T_{\mathrm{eff}}^{*4}$ for a model with effective temperature $T_{\mathrm{eff}}^{*} = 4000\,\mathrm{K}$. After approximately 15 000 s, the instability starts to develop.

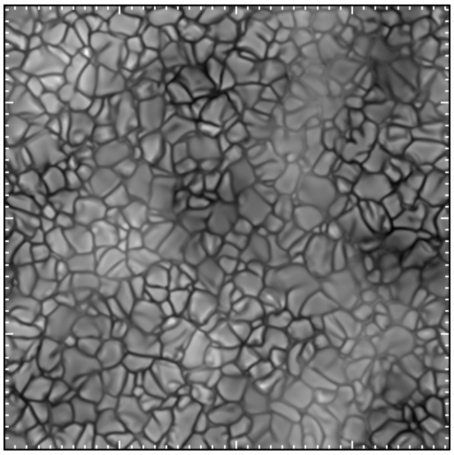

Fig. 6. Vertical velocity at average depth of $\tau_{\mathrm{R}} = 1$ of a solar model with horizontal dimensions 38.4×38.4 Mm. The slowly growing instability is manifest as p-mode patches of high velocities, encompassing several granules. The grayscales extends over approximately $\pm 5\,\mathrm{km\,s^{-1}}$.

One possible remedy consists in closing the bottom boundary, setting the parameters `r0_grav` and `c_coredrag` large enough. When keeping the bottom boundary open, we found as an effective measure to increase the parameter `c_pchange`, which controls the adjustment of the gas pressure in the bottom layers towards the global average (see Freytag et al. 2012; Freytag 2017). Normally, `c_pchange` = 0.3 but we needed to increase this parameter to `c_pchange` = 1.0 for the above mentioned model to bring the slowly growing instability under control. On the other hand, for a model with $T_{\mathrm{eff}}^{*} = 3300\,\mathrm{K}$ and $\log g = 4.5$, a value lower than 0.3 of `c_pchange` seems to mitigate the problem. At this point of time, the new parameters `c_v3changelinbottom` and `c_v3changesqrbottom` (see Freytag 2017) have not yet been ported to the MHD module. Once this has been done, it needs to be checked if the slowly growing instability can be remedied with the help of these parameters alone.

3.3. Miscellaneous

Presently, other miscellaneous minor shortcomings include the items listed below.

i) The present MHD implementation of the FRweno reconstruction scheme assumes equidistance of the grid. It switches back to the (more diffusive) van Leer scheme in any non-equidistant coordinate direction. The MHD module needs yet to be generalized to non-equidistant grids also when invoking FRweno;

ii) The artificial reduction of the Alfvén speed works in conjunction with the internal energy equation only. With the parameter `beta_inv` one can invoke a hybrid scheme under which part of the computational domain in which the magnetic field is weak uses the total energy equation and in parts where it is strong, it uses the internal energy equation. The limits are given by the inverse of the β-parameter, which is the ratio of thermal to magnetic energy density, $\beta = p_{\mathrm{gas}}/(B^2/(8\pi))$. Typical values are `beta_inv` $= 10\ldots100$. With the parameter `va_max`, one can artificially limit the Alfvén speed for the CFL-condition to become more tolerable. In this case, above a certain Alfvén speed, the Lorentz force is reduced by a factor < 1, which is self-consistently taken into account in the energy equation (see also Freytag et al. 2012, and the CO5BOLD user manual under http://www.astro.uu.se/~bf/co5bold).
Both features are purely numerical and independent of each other. However, since the artificial Alfvén-speed reduction works only in conjunction with the internal energy equation, the two parameters are in fact intricately dependent on each other in the sense that the domain of Alfvén-speed reduction must be a subset of the domain of the internal energy equation. In principle, there is no reason why the Alfvén-speed reduction should not also work in conjunction with the total energy equation. It is just not implemented in the current version of the MHD module.

iii) The implemented explicit magnetic diffusion and electric resistivity given by parameters `c_resBconst` and `c_resB` have not been used and tested. They are potentially flawed.

4. Extension in height

To make CO5BOLD fit for an extension of the computational domain into outer atmospheric layers of magnetic stellar atmospheres, more physical processes need to be taken into account. Specifically, these include *(i)* a proper treatment of ohmic dissipation as an energy source for coronal heating, *(ii)* a (Spitzer) heat conductivity which transports heat from the ohmic dissipation sites along the magnetic field. The heat conductivity would have to be numerically treated in a separate (operator splitting) step with an implicit scheme. Steps (i) and (ii) are essential to obtain a proper transition region between the chromosphere and the corona, which in turn is required to take the dynamical boundaries of the chromospheric layer properly into account. For an adequate physical description of the chromosphere, one then should *(iii)* modify the induction equation for the inclusion of a Pedersen resistivity, *(iv)* account for scattering effects in the radiative transfer, and *(v)* account for Hydrogen ionization out of statistical equilibrium. A dynamical Hydrogen ionization is already implemented in the present version of CO5BOLD (see Leenaarts & Wedemeyer-Böhm 2006) but it is exceedingly slow because of the serial (DVODE) ODE solver being used.

Acknowledgements. We are grateful to B. Freytag, H.-G. Ludwig, and M. Steffen for commenting and correcting a draft version of the paper. Thanks are also extended to the referee who helped improving the article. Computations for the simulations of Fig. 3 have been carried out at the Swiss National Supercomputing Centre (CSCS) under project ID s560. This work was supported by the Swiss National Science Foundation under grant ID 200020_157103/1.

References

Calvo, F., Steiner, O., & Freytag, B. 2016, A&A, 596, A43
Freytag, B. 2013, MSAIS, 24, 26
Freytag, B. 2017, MmSAI, 88, 12
Freytag, B., Steffen, M., Ludwig, H.-G., et al. 2012, J. Comp. Phys., 231, 919
Janhunen, P. 2000, J. Comp. Phys., 160, 649
Leenaarts, J. & Wedemeyer-Böhm, S. 2006, A&A, 460, 301
Salhab, R., Steiner, O., Berdyugins, S., et al. 2017, A&A, in preparation
Schaffenberger, W., et al. 2005, in Chromospheric and Coronal Magnetic Fields, ed. D. E. Innes, A. Lagg, & S. A. Solanki, (ESA, Noordwijk), ESA Special Publication, 596, 65.1
Schaffenberger, W., et al. 2006, in Solar MHD Theory and Observations: A High Spatial Resolution Perspective, ed. J. Leibacher, R. F. Stein, & H. Uitenbroek (ASP, San Francisco), ASP Conf. Ser., 354, 345
Steiner, O. & Rezaei, R. 2012, in Fifth Hinode Science Meeting, ed. L. Golub, I. De Moortel, & T. Shimizu (ASP, San Francisco), ASP Conf. Ser. 456, 3
Steiner, O., Rajaguru, S. P., Vigeesh, G., et al. 2013, MSAIS, 24, 100
Steiner, O., Salhab, R., Freytag, B., et al. 2014, PASJ, 66, S5
Vigeesh, G., Jackiewicz, J., & Steiner, O. 2017a, ApJ, 835, 148
Vigeesh, G., Steiner, O., Calvo, F., & Roth, M. 2017b, MmSAI, 88, 54
Wedemeyer, S., Freytag, B., Steffen, M., Ludwig, H.-G., & Holweger, H. 2004, A&A, 414, 1121